

## Properties of the initial participant matter interaction zone in near-Fermi-energy heavy-ion collisions

J. Wang,<sup>\*</sup> T. Keutgen,<sup>†</sup> R. Wada, K. Hagel, S. Kowalski,<sup>‡</sup> T. Materna, L. Qin, Z. Chen, J. B. Natowitz, Y. G. Ma,<sup>§</sup> M. Murray,<sup>||</sup> A. Keksis, E. Martin, A. Ruangma, D. V. Shetty, G. Souliotis, M. Veselsky, E. M. Winchester, and S. J. Yennello

*Cyclotron Institute, Texas A&M University, College Station, Texas 77843, USA*

D. Fabris, M. Lunardon, S. Moretto, G. Nebbia, S. Pesente, V. Rizzi, and G. Viesti  
*INFN and Dipartimento di Fisica dell' Università di Padova, I-35131 Padova, Italy*

M. Cinausero and G. Prete  
*INFN, Laboratori Nazionali di Legnaro, I-35020 Legnaro, Italy*

J. Cibor  
*Institute of Nuclear Physics, ul. Radzikowskiego 152, PL-31-342 Krakow, Poland*

Z. Majka and P. Staszal  
*Jagellonian University, M Smoluchowski Institute of Physics, PL-30059, Krakow, Poland*

W. Zipper  
*Institute of Physics, University of Silesia, PL-40007, Katowice, Poland*

Y. El Masri  
*FNRS and IPN, Université Catholique de Louvain, B-1348 Louvain-Neuve, Belgium*

R. Alfaro, A. Martinez-Davalos, and A. Menchaca-Rocha  
*Instituto de Fisica, Universidad Nacional Autonoma de Mexico, Apactado Postal 20-364 01000, Mexico City, Mexico*

A. Ono  
*Department of Physics, Tohoku University, Sendai 980-8578, Japan*  
(Received 13 March 2006; published 16 January 2007)

The sizes, temperatures, and free neutron-to-proton ratios of the initial interaction zones produced in the collisions of 40 MeV/nucleon  $^{40}\text{Ar} + ^{112}\text{Sn}$  and 55 MeV/nucleon  $^{27}\text{Al} + ^{124}\text{Sn}$  are derived using total detected neutron plus charged particle multiplicity as a measure of the impact parameter range and number of participant nucleons. The size of the initial interaction zone, determined from a coalescence model analysis, increases significantly with decreasing impact parameter. The temperatures and free neutron-to-proton ratios in the interaction zones are relatively similar for different impact parameter ranges and evolve in a similar fashion.

DOI: [10.1103/PhysRevC.75.014604](https://doi.org/10.1103/PhysRevC.75.014604)

PACS number(s): 24.10.-i, 25.70.Gh

### I. INTRODUCTION

For a collision between two heavy nuclei, measurements of emission cross sections for early emitted nucleons and light clusters offer a means to probe the properties and evolution of

the interaction region at early stages of the collision. Because light cluster production in such collisions reflects the particle-particle correlations within this interaction region, detection of a cluster can be viewed as a correlation measurement of its constituent particles in a bound state. Together with suitable application of a coalescence ansatz [1–5], this approach provides information that is complementary to that obtained in particle-particle correlation measurements that are well established in the nuclear context and have been applied in a wide range of studies [6,7]. We have previously applied these techniques to obtain information on the early reaction dynamics and on the thermal evolution of the hot nuclei produced in near-Fermi-energy heavy-ion collisions [8–12]. In this article we report on the use of coalescence model analyses of light particle emission to probe the impact parameter dependence of

<sup>\*</sup>Now at Institute of Modern Physics Chinese Academy of Science, Lanzhou 73, China.

<sup>†</sup>Now at FNRS and IPN, Université Catholique de Louvain, B-1348 Louvain-Neuve, Belgium.

<sup>‡</sup>Now at Institute of Physics, Silesia University, Katowice, Poland.

<sup>§</sup>On leave from Shanghai Institute of Nuclear Research, Chinese Academy of Sciences, Shanghai 201800, China.

<sup>||</sup>Now at University of Kansas, Lawrence, KS 66045-7582.

the properties of the initial interaction zone and the evolution of participant matter produced in collisions of 40 MeV/nucleon  $^{40}\text{Ar} + ^{112}\text{Sn}$  and 55 MeV/nucleon  $^{27}\text{Al} + ^{124}\text{Sn}$ . We find that the size of the initial interaction zone increases significantly with decreasing impact parameter. The temperatures and free neutron-to-proton ratios in the interaction zones are relatively similar for different impact parameter ranges and they evolve in a similar fashion.

## II. EXPERIMENT

The reactions 40 MeV/nucleon  $^{40}\text{Ar} + ^{112}\text{Sn}$  and 55 MeV/nucleon  $^{27}\text{Al} + ^{124}\text{Sn}$  were studied at the K-500 superconducting cyclotron facility at Texas A&M University. For these studies we used the NIMROD detector array consisting of a  $4\pi$  charged-particle array inside a  $4\pi$  neutron calorimeter [13,14]. The charged-particle detector array of NIMROD includes 166 individual CsI detectors arranged in 12 rings in polar angles from  $\sim 4^\circ$  to  $\sim 160^\circ$ . In these experiments Si-CsI telescopes were used to identify intermediate mass fragments (IMF). For the present experiment each forward ring also included two “supertelescopes,” each containing two Si  $\Delta E$  detectors and a CsI E detector and seven telescopes containing a single Si  $\Delta E$  detector and a CsI E detector. Neutron multiplicity was measured with the  $4\pi$  neutron detector surrounding the charged-particle array. This detector is a neutron calorimeter filled with a gadolinium-doped pseudocumene liquid scintillator. Thermalization and capture of emitted neutrons leads to scintillation that is observed with phototubes providing event-by-event determinations of neutron multiplicity but little information on neutron energies and angular distributions. Further details on the detection system, energy calibrations, and neutron calorimeter efficiency may be found in Ref. [13]. During the experiment, data were taken employing two different trigger modes, one a minimum bias trigger in which at least one of the CsI detectors detected a particle and the other a high-multiplicity trigger that required detected particles in three to five CsI detectors (depending on the reaction studied). We previously reported on excitation energy deposition and composite nucleus de-excitation in the most violent collisions observed for these systems [12].

## III. DATA ANALYSIS

Many of the techniques applied in this analysis were discussed previously in greater detail in Refs. [8–13,15]. Only a brief summary of these techniques is included in the present work.

For the reaction systems studied, an inspection of the two-dimensional arrays depicting the detected correlation between charged-particle multiplicity and neutron multiplicity in NIMROD reveals a distinct correlation in which increasing charged-particle multiplicity is associated with increasing neutron multiplicity.

Although there are significant multiplicity fluctuations reflecting both the competition between the different decay modes and the instrumental detection efficiencies, the data show that the total number of emitted particles can serve as a

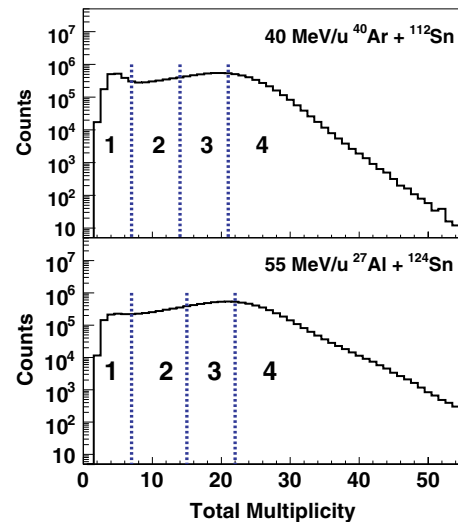


FIG. 1. (Color online) Total detected multiplicity of charged particles and neutrons observed with the NIMROD detector. Dashed lines indicate the multiplicity bins selected for the analysis. (a) 40 MeV/nucleon  $^{40}\text{Ar} + ^{112}\text{Sn}$  (b) 55 MeV/nucleon  $^{27}\text{Al} + ^{124}\text{Sn}$ .

useful means for categorizing collisions according to impact parameter range. Simulations with the AMD-V transport code [16] lead to similar conclusions. For the two reactions considered, the experimental distributions of total neutron plus charged particle multiplicity are shown in Fig. 1. For the analysis reported in this article we have used the total combined charged particle plus neutron multiplicities to select event classes for further analysis. For each of the reactions, events corresponding to four different regions of observed total detected neutron plus charged particle multiplicity were selected for analysis. These regions in total multiplicity are indicated by the dashed lines in Fig. 1.

For the events in each selected multiplicity region we then carried out analyses using three-source fits to the observed energy and angular distributions of the light charged particles. The assumed sources were the PLF (projectile-like fragment) source, the targetlike fragment source (TLF), and an intermediate velocity (IV) source [4,12,17–19]. From these fits we obtained parameters describing the ejectile spectra and multiplicities that can be associated to the three different sources. For the reactions studied, the spectral parameters for of  $^1\text{H}$ ,  $^2\text{H}$ ,  $^3\text{H}$ ,  $^3\text{He}$ , and  $^4\text{He}$  emission from the different sources, derived from the fits, follow the trends of earlier reported values at such projectile energies [4,12,17–20]. The IV source slope parameters for  $^1\text{H}$ ,  $^2\text{H}$ ,  $^3\text{H}$ ,  $^3\text{He}$ , and  $^4\text{He}$  are characteristic of those for pre-equilibrium emission in this projectile energy range [12,17–22]. Given the continuous dynamic evolution of the system, such source fits should be considered as providing only a schematic picture of the emission process. We have employed them to estimate the multiplicities and energies of ejectiles emitted at each stage of the reaction for each region of multiplicities. Both the mass of light ejectiles associated with the IV source and that associated with the TLF source increase monotonically with increasing total multiplicity. In the following we shall be particularly interested in the properties of the ejectiles from the IV

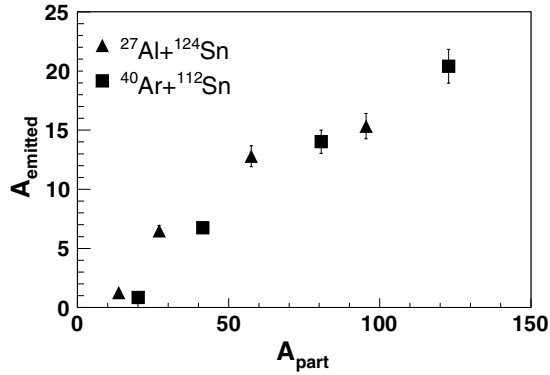


FIG. 2. Mass emitted from the IV source as nucleons and light clusters plotted as a function of  $A_{\text{part}}$  determined from Glauber model calculations. Results are presented for 40 MeV/nucleon  $^{40}\text{Ar} + ^{112}\text{Sn}$  (solid squares) and 55 MeV/nucleon  $^{27}\text{Al} + ^{124}\text{Sn}$  (solid diamonds).

source. To explore this part of the emission further, we have employed the Glauber model of Ref. [23] to estimate the number of participating nucleons corresponding to the different selected bins in total multiplicity. For this purpose a sharp cut-off approximation was employed to divide the results of the Glauber model calculation into four impact parameter bins, ranging from peripheral to central. These bins were matched to the bins employed for the experimental data by assuming that increasing total multiplicity corresponds to decreasing impact parameter and choosing the impact parameter ranges for each bin to assure that it contained an identical fraction of the total reaction cross section to that of the corresponding experimental sample. For each bin the average number of participant nucleons,  $A_{\text{part}}$ , was then determined from the Glauber model calculation. In Fig. 2 we present the relationship between the average numbers of participating nucleons and the yields of ejectiles for emission from the IV source. For both systems, the mass yield is seen to increase monotonically with  $A_{\text{part}}$ , confirming the strong correlation between the number of participants and the number of early emitted particles. This reflects the early collision dynamics within the initial interaction zone containing the participant matter from the two collision partners.

In the following we attempt to probe further into the nature of this initial participant zone.

#### IV. PARTICIPANT ZONE PROPERTIES

To probe the properties of the initial interaction zone, i.e., the sizes, temperatures, and  $N/Z$  ratios of these zones, we have applied coalescence model analyses [1–3]. In coalescence models the yields of ejected light clusters are directly related to the free nucleon yields. The phase-space correlations that lead to cluster formation may be parametrized in terms of the momentum-space volume within which the correlations between nucleons exist. This momentum-space volume is assumed to be spherical with a radius of  $P_0$ . Analysis of the nucleon and cluster yields and extraction of  $P_0$  provide information on the properties of the emission zone.

To determine the coalescence parameter,  $P_0$ , in our energy range we have followed the Coulomb corrected coalescence model formalism of Awes *et al.* [4] for which the laboratory frame differential yield for a cluster of  $Z$  protons and  $N$  neutrons, having mass number  $A$  and a Coulomb-corrected energy per nucleon  $E_A$  is:

$$\frac{d^2N(Z, N, E_A)}{dE_A d\Omega} = \left( \frac{N_t + N_p}{Z_t + Z_p} \right)^N \frac{A^{-1}}{N!Z!} \times \left( \frac{\frac{4}{3}\pi P_0^3}{[2m^3(E - E_c)]^{\frac{1}{2}}} \right)^{A-1} \times \left[ \frac{d^2N(1, 0, E)}{dE d\Omega} \right]^A \quad (1)$$

where  $t$  denotes the target nucleus and  $p$  the projectile nucleus.

This cluster yield is directly related to the proton double differential yield at the same energy per nucleon,  $E$ , i.e., at the same velocity. The energy prior to Coulomb acceleration is obtained in the analysis by subtraction of the Coulomb barrier energy,  $E_c$ , derived from the source fits. Because the system size may evolve during the particle emission stage we derive the parameter  $P_0$  as a function of velocity as in previous works [8–12]. The velocity we employ is the “surface velocity,”  $V_{\text{surf}}$ , of the emitted particle, defined as the velocity of an emitted species at the nuclear surface, prior to acceleration in the Coulomb field [4]. In this work  $V_{\text{surf}}$  is determined from the particle energy by subtracting the effective Coulomb energy determined from the source fits. To focus on the earlier evolution of the system we also subtracted the contributions from the TLF source from the total spectra. This was done using the experimentally determined fit parameters for the TLF source. Because the early emitted light particle energies are strongly correlated with emission times, and the evaporative or secondary emission contributions to the spectra are primarily at the lower kinetic energies, the yields of higher energy particles are relatively uncontaminated by later emission processes. To further focus on early particle emission we chose to work in the IV source frame and define  $V_{\text{surf}}$  as the surface velocity in that frame. In that IV frame we selected nucleons and clusters emitted at midrapidity, i.e., at angles of  $70^\circ$  to  $80^\circ$  in the IV source frame. In this way we attempted to isolate the emission associated with the IV source that occurs during the thermalization stage of the reaction by minimizing contributions from the PLF and TLF sources.

These two techniques are quite useful in discriminating against secondary decay contributions. To put this on a somewhat more quantitative basis we have used various experimental results from the literature to evaluate the magnitude of secondary decay contributions to systems such as those we investigate [13,24–30]. Briefly, for the more central collisions, these results indicate that  $\sim 10\%$  of the total observed light charged particle emission comes from secondary decay. This emission dominates the yields at later times, i.e., that associated primarily with the TLF source that we attempt to remove by subtraction from the data. This TLF source may consist of one or more excited intermediate mass fragments (IMFs) that are undergoing secondary decay. In systems such

as ours, in addition to a heavy composite nucleus, an average IMF multiplicity of  $\sim 1$  to 1.5 is expected [13,24,27–29]. The IMFs are typically excited to  $\sim 3$  MeV/nucleon and average multiplicities of emission from such IMFs have been determined experimentally [13,25,26]. Using the information in the cited references we estimate that secondary decay from the IMFs contributes  $\sim 22, 14, 9, 4,$  and  $34\%$ , respectively, of the total  $p, d, t, {}^3\text{He},$  and  ${}^4\text{He}$  secondary decays. To the extent that the IMFs are associated with the TLF source this contribution should be removed by the subtraction technique we employ. Contributions from decay of any IMFs moving with velocities comparable to that of the IV source would not be excluded in our analysis. Such fragments do not appear to be important in the more central collisions [13,30] but may be more likely in peripheral and midperipheral collisions.

### V. ${}^3\text{H}/{}^3\text{He}$ RATIOS AND $n/p$ RATIOS

As indicated by Eq. (1), in this coalescence model the ratios of two isotopes that differ by one neutron are essentially determined by the ratio of “free nucleons” in the coalescence volume. Thus, the free  $n/p$  ratio can be determined from a measurement of the  ${}^3\text{H}/{}^3\text{He}$  ratio [31,32]. In Fig. 3 we present measured values of the  ${}^3\text{H}/{}^3\text{He}$  ratio as a function of  $V_{\text{surf}}$ .

Except at the very highest velocities, these ratios are seen to be significantly higher than the total  $N/Z$  ratios in the entrance channel (1.24 for  ${}^{40}\text{Ar} + {}^{112}\text{Sn}$  and 1.40 for  ${}^{27}\text{Al} + {}^{124}\text{Sn}$ ). This is consistent with earlier results obtained by Albergo *et al.* [33], who deduced significant free neutron excesses based on integrated yields observed in a variety of early intermediate energy experiments. Other recent work also results in large  ${}^3\text{H}/{}^3\text{He}$  ratios [9,34,35]. It has been suggested that such observations provide evidence for a distillation leading to a nucleon vapor that is enriched in neutrons relative to a coexisting nuclear liquid in accordance with predictions of several theoretical studies [36,37]. However, Sobotka *et al.*

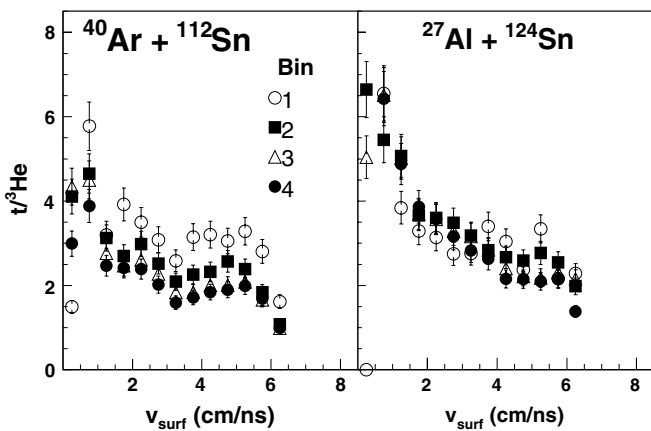


FIG. 3.  ${}^3\text{H}/{}^3\text{He}$  ratios as a function of surface velocity. Symbols of open circles, solid squares, open triangles, and solid circles correspond, respectively, to progressively increasing total neutron plus charged particle multiplicity. (a) 40 MeV/nucleon  ${}^{40}\text{Ar} + {}^{112}\text{Sn}$ ; (b) 55 MeV/nucleon  ${}^{27}\text{Al} + {}^{124}\text{Sn}$ . See text and Fig. 1 for details.

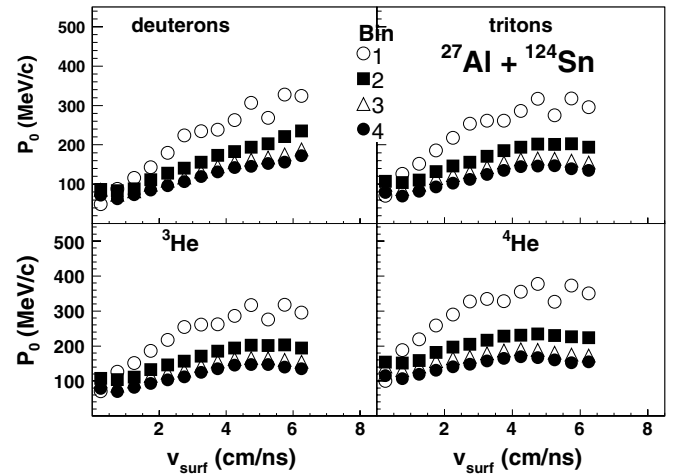


FIG. 4.  $P_0$  as a function of  $V_{\text{surf}}$  for 55 MeV/nucleon  ${}^{27}\text{Ar} + {}^{124}\text{Sn}$ . Results are presented for  ${}^2\text{H}$  (upper left),  ${}^3\text{H}$  (upper right),  ${}^3\text{He}$  (lower left), and  ${}^4\text{He}$  (lower right). In each case data are presented for four selected windows. Symbols of open circles, solid squares, open triangles, and solid circles correspond, respectively, to progressively increasing total neutron plus charged particle multiplicity. See text.

have pointed out that symmetric cluster formation may play an important role in determining these ratios [38].

### VI. COALESCENCE PARAMETERS, $P_0$

Using the observed  ${}^3\text{H}/{}^3\text{He}$  ratios to determine the  $n/p$  ratios required in Eq. (1), we have calculated the coalescence radius,  $P_0$ , as a function of  $V_{\text{surf}}$ . It should be noted that the method of derivation of the  $N/Z$  ratio from the  ${}^3\text{H}$  to  ${}^3\text{He}$  ratio leads to identical  $P_0$  values for  ${}^3\text{H}$  and  ${}^3\text{He}$ . The results, presented in Fig. 4 and Fig. 5 reveal that, for each light cluster, the derived values of  $P_0$  decrease with decreasing  $V_{\text{surf}}$  and also

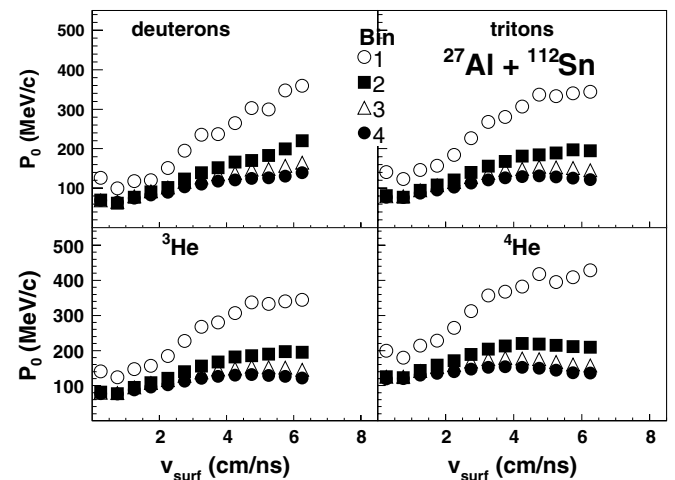


FIG. 5.  $P_0$  as a function of  $V_{\text{surf}}$  for 40 MeV/nucleon  ${}^{40}\text{Ar} + {}^{112}\text{Sn}$ . Results are presented for  ${}^2\text{H}$  (upper left),  ${}^3\text{H}$  (upper right),  ${}^3\text{He}$  (lower left), and  ${}^4\text{He}$  (lower right). In each case data are presented for four selected windows. Symbols of open circles, solid squares, open triangles, and solid circles correspond, respectively, to progressively increasing total ejectile multiplicity. See text.

decrease with increasing total neutron plus charged particle multiplicity. A closer inspection shows that the trend with surface velocity appears somewhat different for deuterons than for the other clusters. We also see a tendency for  $P_0$  values for  $\alpha$  particles in a given multiplicity bin to be larger than the values for the other clusters.

## VII. INTERACTION ZONE SIZES

To extract nuclear size information from the  $P_0$  measurements, the thermal coalescence model of Mekjian [2] has been employed. In the Mekjian model there is a direct relationship between the volume in momentum space and the coordinate space volume of the emitting system. In terms of the  $P_0$  derived from Eq. (1) the relationship is:

$$V = \left[ \left( \frac{Z!N!A^3}{2^A} \right) (2s+1) e^{\frac{E_0}{T}} \right]^{\frac{1}{(A-1)}} \frac{3h^3}{4\pi P_0^3}, \quad (2)$$

where  $Z$ ,  $N$ , and  $A$  have the same meaning as in Eq. (1),  $E_0$  is the binding energy,  $s$  is the spin of the emitted cluster, and  $T$  is the temperature. Thus in the coalescence model ansatz the volume of the emitting system can be derived from  $P_0$ . For this purpose, the temperature must be determined. Assuming a spherical shape of uniform density, the configuration space radius,  $R_0$ , may then be derived. This model assumes that both chemical and thermal equilibrium are achieved. Thus its applicability must be evaluated using a variety of experimental observables. In our previous work on similar systems, we have concluded that the data are consistent with achievement of such an equilibration, at least on a local basis [11,12]. This point is discussed further in the following section.

## VIII. DOUBLE ISOTOPE RATIO TEMPERATURES

In an equilibrium model framework, the temperatures may be evaluated from double isotope yield ratio measurements [2,11,12,33]. Using the same techniques as in Refs. [11,12] we determined, the double isotope yield ratio temperatures,  $T_{\text{HHe}}$ , derived from the yields of  ${}^2\text{H}$ ,  ${}^3\text{H}$ ,  ${}^3\text{He}$ , and  ${}^4\text{He}$  clusters. This has been done as a function of ejectile velocity for each total multiplicity window for the two different systems under consideration. For particles emitted from a single source of temperature,  $T$ , and having a volume Maxwellian spectrum,  $\epsilon^{\frac{1}{2}} e^{-\epsilon/T}$ , where  $\epsilon$  is the particle energy. The HHe double isotope yield ratio evaluated for particles of equal  $V_{\text{surf}}$ , is  $(9/8)^{1/2}$  times the ratio derived from either the integrated particle yields or the yields at a given energy above the barrier [11]. Thus

$$T_{\text{HHe}} = \frac{14.3}{\ln[\sqrt{(9/8)}(1.59R_{V_{\text{surf}}})]}. \quad (3)$$

If  $Y$  represents a cluster yield,  $R_{V_{\text{surf}}} = Y({}^2\text{H})Y({}^4\text{He})/Y({}^3\text{H})Y({}^3\text{He})$  for clusters with the same surface velocity and the constants 14.3 and 1.59 reflect binding energy, spin, masses, and mass differences of the ejectiles. Equation (3) differs from the usual formulation by a factor of  $(9/8)^{1/2}$  appearing in the logarithm term in the denominator [33].

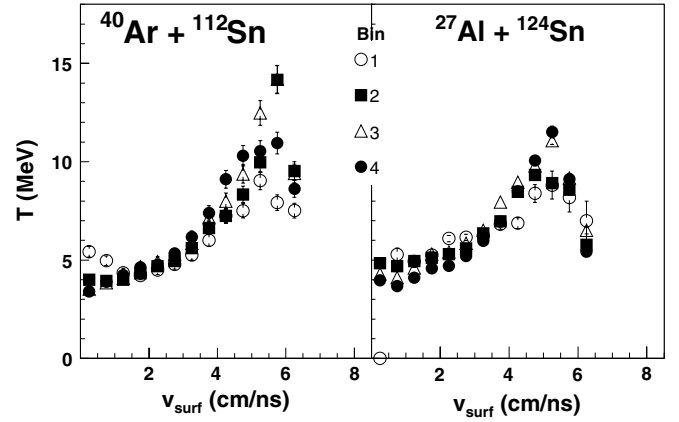


FIG. 6. Evolution with surface velocity of the double isotope ratio temperature,  $T_{\text{HHe}}$  for the two different reactions, 40 MeV/nucleon  ${}^{40}\text{Ar} + {}^{112}\text{Sn}$ - and 55 MeV/nucleon  ${}^{27}\text{Al} + {}^{124}\text{Sn}$ . Symbols of open circles, solid squares, open triangles, and solid circles correspond, respectively, to progressively increasing total neutron plus charged particle multiplicity. See text.

We present, in Fig. 6, the resultant double isotope ratio temperatures,  $T_{\text{HHe}}$ , as a function of surface velocity. For the most violent collisions the temperature results have previously been reported [12]

In Fig. 6 we see that as  $V_{\text{surf}}$  decreases from the highest  $V_{\text{surf}}$  sampled, i.e., as reaction time increases, each of the temperature evolution curves exhibits a maximum and then decreases. Maximum temperatures of 8–14 MeV are observed. The trends in Fig. 6 are very similar to those reported for previous measurements of the temperature evolution in the reactions of 26–47 MeV/nucleon projectiles with various targets [8,9,11,12]. In those works the correlation of decreasing surface velocity with increasing mean emission time is discussed and the evolution times are estimated. In Ref. [11] the peaks in the temperature at surface velocities near 6 cm/ns were interpreted as implying times in the range of 95 to 110 fm/c, depending on the reaction system. After that time the temperature decreases monotonically with decreasing surface velocity. It should be emphasized that large thermal fluctuations prevent the direct association of a particular velocity with a particular emission time. Thus the times being determined are weighted averages for particles of a certain velocity. It is further assumed, within the coalescence assumption, that clusters of a certain surface velocity are formed from nucleons having the same surface velocity. AMD-V model calculations [11–13,16] for those systems indicate a significant slowing in the rate of change of the ejectile kinetic energy near a velocity of 3.5 cm/ns, signaling the end of the IV (or pre-equilibrium) emission stages and entry into the region of slower nuclear de-excitation modes, i.e., evaporation, fission, and/or fragmentation. At that point the sensitivity of the emission energy to time is significantly reduced. Consequently, we take the temperature at the time corresponding to the velocity of 3.5 cm/ns to be that of the hot nucleus at the beginning of the final statistical emission stage (appropriate to initial emission from the TLF source.) At that point the corresponding  $T_{\text{HHe}}$  temperatures are near 6 MeV and thus very similar to the limiting temperatures

previously derived from a systematic investigation of caloric curve measurements [39] in this mass region. In Ref. [11,12] it is concluded that for velocities below those corresponding to the peaks in the temperature curves, the temperature data are consistent with the achievement of chemical and thermal equilibration, at least as sampled on a local basis.

**IX. EMISSION ZONE RADII**

As indicated in the previous section, once the temperatures are available, emission zone radii may be determined from the  $P_0$  values. We previously observed that the radii derived from the different clusters are slightly different [9]. Those derived from the deuteron yields are larger, and those derived from  $\alpha$ -particle yields are lower than those derived from  $^3\text{H}$  and  $^3\text{He}$ . The same is true in the present work, as is indicated in Fig. 7. These differences may reflect real differences in the densities of the last interaction, i.e., in the survivability [22] of these clusters that can result from binding energy differences. That is, the radius of the surface of the last nondestructive interaction of the strongly bound  $\alpha$  particle may be less than that of the weakly bound deuteron.

For the present work we have chosen to derive average values of  $R_0$  obtained from the four different ejectiles. These are presented in Fig. 8 for the four different windows of total neutron plus charged particle multiplicity. The errors are estimated systematic uncertainties in the final results.

Over the range of  $V_{\text{surf}}$  from 3 to 6 cm/ns these values are averaged for 1-cm/ns intervals. Here the observed trends in  $P_0$  result in a significant increase in  $R_0$  with increasing total neutron plus charged particle multiplicity. The derived values of  $R_0$  are seen to range from  $\sim 2.5$  to  $\sim 7.5$  F and be rather similar for the two systems. For the most violent

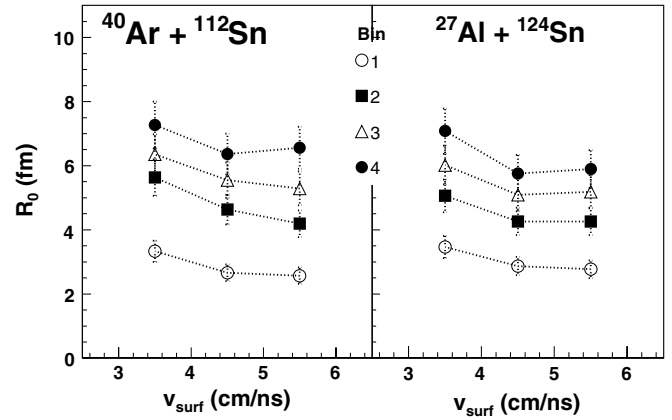


FIG. 8. Interaction zone radii as a function of  $V_{\text{surf}}$ . Values averaged over bins of 1 cm/ns in  $V_{\text{surf}}$  are presented for four different windows of total neutron plus charged particle multiplicity for the systems (a) 40 MeV/nucleon  $^{40}\text{Ar} + ^{112}\text{Sn}$  and (b) 55 MeV/nucleon  $^{27}\text{Al} + ^{124}\text{Sn}$ . Symbols of open circles, solid squares, open triangles, and solid circles correspond, respectively, to progressively increasing total neutron plus charged particle multiplicity.

collisions, values of  $R_0$  at the highest surface velocities are 6 to 6.5 F, close to the expectations for the equivalent sharp cut-off radius of normal density nuclei with total mass numbers equal to those of the entrance channel,  $A = 151$  or  $152$  [40]. An increase of  $R_0$  with decreasing velocity is seen for the different impact parameter windows. The fractional changes for different windows are quite similar.

To further evaluate the evolution of the interaction zone size, we have explored the correspondence between interaction zone size and the number of participant nucleons. For this purpose we have adopted a somewhat different estimate of the later quantity by relaxing the sharp cut-off approximation of the Glauber model estimate. As previous calculations employing the AMD model of Ono *et al.* [16] were found to reproduce well a variety of experimental observables for similar systems, we filtered results of AMD calculations for the two systems using the same conditions as employed for the experimental data. Not unexpectedly these results indicated that the impact parameter ranges selected by the adopted windows in total charged particle plus neutron multiplicity are not as sharply defined as those used to determine the average  $A'_{\text{part}}$  of the Glauber model. We then revised these estimates of  $A'_{\text{part}}$  by weighting the Glauber model results by the derived AMD impact parameter distributions. This procedure results in estimates of the participating nucleon numbers that are 10% lower than those obtained with the sharp cut-off assumption. In Figs. 9(a)–9(c) the derived radii are plotted against these refined estimates, designated  $A'_{\text{part}}$ . For comparison, fits of the function  $R_0 = r_0(A'_{\text{part}})^{1/3}$  are also shown. This function fits the data reasonably. The values of  $r_0$  extracted from these fits increase with decreasing surface velocity. They are 1.27, 1.28, and 1.51 fm, respectively, for the 5 to 6-, 4 to 5-, and 3 to 4-cm/ns windows. The scaling clearly implies that the size of the zone being sampled is proportional to  $A'_{\text{part}}$ . If the zone contains  $A'_{\text{part}}$  nucleons and has a spherical shape, a comparison of the  $r_0$  values with the equivalent uniform radius parameter

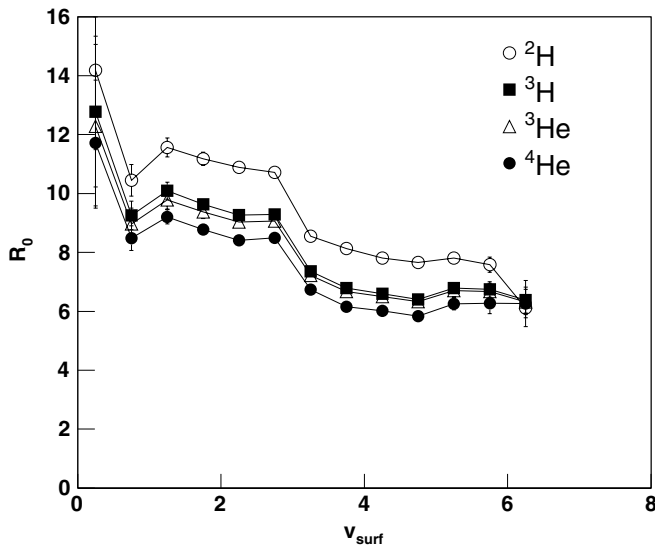


FIG. 7. Interaction zone radii as a function of  $V_{\text{surf}}$ . Values are presented for the four different ejectiles from the system 55 MeV/nucleon  $^{27}\text{Al} + ^{124}\text{Sn}$ . Symbols of open circles, solid squares, open triangles, and solid circles correspond, respectively, to data for  $^2\text{H}$ ,  $^3\text{H}$ ,  $^3\text{He}$ , and  $^4\text{He}$ , respectively. A similar trend is seen for 40 MeV/nucleon  $^{40}\text{Ar} + ^{112}\text{Sn}$ .

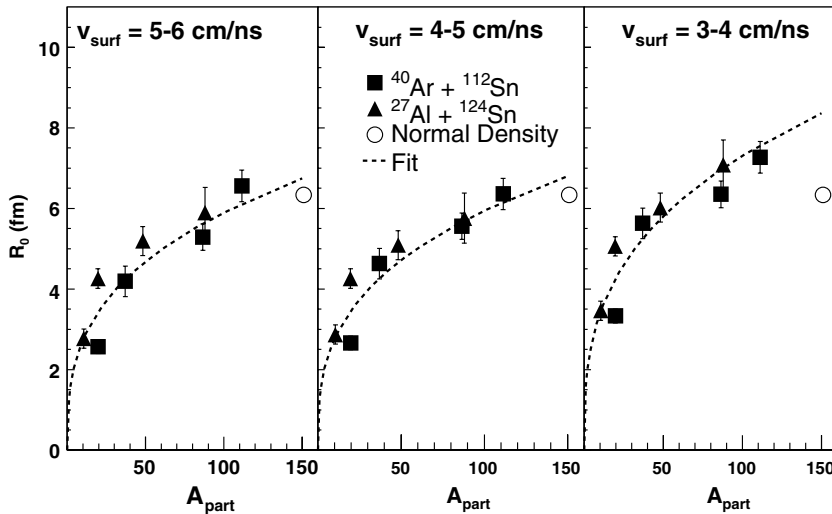


FIG. 9. Emission zone radii vs.  $A'_{\text{part}}$  (see text) for three different windows on  $V_{\text{surf}}$ . Results for both reactions are presented as average values of  $R_0$  for three bins of 1 cm/ns in  $V_{\text{surf}}$  in the range of 3 to 6 cm/ns. Average values of  $V_{\text{surf}}$  are (a) 5.5 cm/ns, (b) 4.5 cm/ns, and (c) 3.5 cm/ns. Symbols are as follows: solid triangles, 55 MeV/nucleon  $^{27}\text{Al} + ^{124}\text{Sn}$ , and solid squares, 40 MeV/nucleon  $^{40}\text{Ar} + ^{112}\text{Sn}$ . For comparison, the equivalent sharp cut-off radius for a normal density nucleus with  $A = 151$  is indicated by the open circles in each part of the figure.

for normal density nuclei with  $A = 151$  [40], indicated by an open circle in each part of Fig. 9, would suggest corresponding average densities decreasing from  $0.85\rho_0$  to  $0.50\rho_0$  (where  $\rho_0$  is the normal ground-state nuclear density) as the system evolves and  $V_{\text{surf}}$  decreases. Such average density estimates are close to those derived from a Fermi gas model analysis of caloric curves for similar systems [41].

However, given that (1) many collisions should be Pauli blocked, that (2) some nucleons are emitted during this process, and that (3) thermalization is occurring, it is difficult to extract precise information on the densities. Indeed, the AMD calculations for these and similar systems clearly indicate large density fluctuations with fragments of normal density imbedded in a lower-density medium of nucleons and smaller clusters, a nuclear gas [13,16]. Thus the system under investigation is far from being a uniform density expanding and evaporating system as is often assumed. If the nuclear gas is equated to the early emitted particles from the IV source, the observed scaling with  $A_{\text{part}}^{1/3}$  may simply reflect the direct dependence of the total mass of the emitted particles on the number of participant nucleons that is seen in Fig. 2. In such a case, the interaction zone radii extracted from the coalescence model might better be viewed as those characterizing the nuclear gas and the densities derived from the ratios of the number of gas nucleons to the interaction zone radii would near  $0.1\rho_0$ . If this latter interpretation proves to be correct, it may be possible to employ analyses of such reaction data to test theoretical predictions of the properties of low-density nuclear gases [42–44] in greater detail.

## X. SUMMARY AND CONCLUSIONS

The sizes, temperatures, and free neutron to proton ratios of the initial interaction zones produced in the collisions of 40 MeV/nucleon  $^{40}\text{Ar} + ^{112}\text{Sn}$  and 55 MeV/nucleon  $^{27}\text{Al} + ^{124}\text{Sn}$  are derived for different total multiplicities of emitted neutrons and charged particles. The size of the initial interaction zone, derived from coalescence model analyses, increases significantly with total neutron plus charged particle multiplicity ( $\sim$ centrality). The temperatures and the free neutron-to-proton ratios in these zones exhibit very similar evolutions with decreasing surface velocity. The similar behavior of these observables with surface velocity for the different bins indicates that the thermal and chemical properties of the participant zones are very similar from the most peripheral to the most central collisions. The interaction zone radii obtained from the coalescence analyses have been found to correlate well with the number of nucleons in the participant matter region. The interpretation of this correlation is discussed and it is suggested that measurements of the type reported here may allow more detailed investigation of the properties of low density nuclear gases, a topic of both nuclear and astrophysical interest [42–44]. We are currently exploring this possibility.

## ACKNOWLEDGMENTS

This work was supported by the United States Department of Energy under grant DE-FG03-93ER40773 and by The Robert A. Welch Foundation under grants A0330 and A1266.

- [1] L. P. Csernai and J. I. Kapusta, Phys. Rep. **131**, 223 (1986).
- [2] A. Z. Mekjian, Phys. Rev. C **17**, 1051 (1978); Phys. Rev. Lett. **38**, 640 (1977); Phys. Lett. **B89**, 177 (1980).
- [3] H. Sato and K. Yazaki, Phys. Lett. **B98**, 153 (1981).
- [4] T. C. Awes, G. Poggi, C. K. Gelbke, B. B. Back, B. G. Glagola, H. Breuer, and V. E. Viola, Jr., Phys. Rev. C **24**, 89 (1981).
- [5] W. J. Llope, S. E. Pratt, N. Frazier, R. Pak, D. Craig, E. E. Gualtieri, S. A. Hannuschke, N. T. B. Stone, A. M. Vander Molen, G. D. Westfall, J. Yee, R. A. Lacey, J. Lauret,

- A. C. Mignerey, and D. E. Russ, Phys. Rev. C **52**, 2004 (1995).
- [6] W. Bauer, C. K. Gelbke, and S. Pratt, Annu. Rev. Nucl. Part. Sci. **42**, 77 (1992).
- [7] D. Ardouin, Int. J. Mod. Phys. E **6**, 391 (1997).
- [8] J. Cibor, R. Wada, K. Hagel, M. Lunardon, N. Marie, R. Alfaro, W. Q. Shen, B. Xiao, Y. Zhao, J. Li, B. A. Li, M. Murray, J. B. Natowitz, Z. Majka, and P. Staszal, Phys. Lett. **B473**, 29 (2000).

- [9] K. Hagel, R. Wada, J. Cibor, M. Lunardon, N. Marie, R. Alfaro, W. Shen, B. Xiao, Y. Zhao, Z. Majka, J. Li, P. Staszal, B.-A. Li, M. Murray, T. Keutgen, A. Bonasera, and J. B. Natowitz, *Phys. Rev. C* **62**, 034607 (2000).
- [10] J. Cibor, A. Bonasera, J. B. Natowitz, R. Wada, K. Hagel, M. Murray, and T. Keutgen, in *Isospin Physics in Heavy-Ion Collisions at Intermediate Energies*, edited by Bao-An Li and W. Udo Schroeder (NOVA Science, New York, 2001).
- [11] J. Wang, R. Wada, T. Keutgen, K. Hagel, Y. G. Ma, M. Murray, L. Qin, A. Botvina, S. Kowalski, T. Materna, J. B. Natowitz, R. Alfaro, J. Cibor, M. Cinausero, Y. El Masri, D. Fabris, E. Fioretto, A. Keksis, M. Lunardon, A. Makeev, N. Marie, E. Martin, Z. Majka, A. Martinez-Davalos, A. Menchaca-Rocha, G. Nebbia, G. Prete, V. Rizzi, A. Ruangma, D. V. Shetty, G. Souliotis, P. Staszal, M. Veselsky, G. Viesti, E. M. Winchester, S. J. Yennello, W. Zipper, and A. Ono, *Phys. Rev. C* **72**, 024603 (2005).
- [12] J. Wang, T. Keutgen, R. Wada, K. Hagel, Y. G. Ma, M. Murray, L. Qin, P. Smith, J. B. Natowitz, R. Alfaro, J. Cibor, A. Botvina, M. Cinausero, Y. El Masri, D. Fabris, A. Keksis, S. Kowalski, M. Lunardon, A. Makeev, N. Marie, E. Martin, Z. Majka, A. Martinez-Davalos, A. Menchaca-Rocha, G. Nebbia, S. Moretto, G. Prete, V. Rizzi, A. Ruangma, D. V. Shetty, G. Souliotis, P. Staszal, M. Veselsky, G. Viesti, E. M. Winchester, S. J. Yennello, W. Zipper, and A. Ono, *Phys. Rev. C* **71**, 054608 (2005).
- [13] R. Wada, T. Keutgen, K. Hagel, Y. G. Ma, J. Wang, M. Murray, L. Qin, P. Smith, J. B. Natowitz, R. Alfaro, J. Cibor, M. Cinausero, Y. El Masri, D. Fabris, E. Fioretto, A. Keksis, M. Lunardon, A. Makeev, N. Marie, E. Martin, A. Martinez-Davalos, A. Menchaca-Rocha, G. Nebbia, G. Prete, V. Rizzi, A. Ruangma, D. V. Shetty, G. Souliotis, P. Staszal, M. Veselsky, G. Viesti, E. M. Winchester, S. J. Yennello, Z. Majka, and A. Ono, *Phys. Rev. C* **69**, 044610 (2004).
- [14] R. P. Schmitt, L. Cooke, G. Derrig, D. Fabris, B. Hurst, J. B. Natowitz, G. Nebbia, D. O'Kelly, B. Srivastava, B. Turmel, D. Utley, H. Utsonomiya, and R. Wada, *Nucl. Instrum. Methods A* **354**, 487 (1995).
- [15] Y. G. Ma, J. B. Natowitz, R. Wada, K. Hagel, J. Wang, T. Keutgen, Z. Majka, M. Murray, L. Qin, P. Smith, R. Alfaro, J. Cibor, M. Cinausero, Y. El Masri, D. Fabris, E. Fioretto, A. Keksis, M. Lunardon, A. Makeev, N. Marie, E. Martin, A. Martinez-Davalos, A. Menchaca-Rocha, G. Nebbia, G. Prete, V. Rizzi, A. Ruangma, D. V. Shetty, G. Souliotis, P. Staszal, M. Veselsky, G. Viesti, and E. M. Winchester, *Phys. Rev. C* **71**, 054606 (2005).
- [16] A. Ono, *Phys. Rev. C* **59**, 853 (1999).
- [17] T. C. Awes, G. Poggi, C. K. Gelbke, B. B. Back, B. G. Glagola, H. Breuer, and V. E. Viola, Jr., *Phys. Rev. C* **24**, 89 (1981).
- [18] D. Prindle, A. Elmaani, C. Hyde-Wright, W. Jiang, A. A. Sonzogni, R. Vandenbosch, D. Bowman, G. Cron, P. Danielewicz, J. Dinius, W. Hsi, W. G. Lynch, C. Montoya, G. Peaslee, C. Schwarz, M. B. Tsang, C. Williams, R. T. deSouza, D. Fox, and T. Moore, *Phys. Rev. C* **57**, 1305 (1998).
- [19] R. Wada, D. Fabris, K. Hagel, G. Nebbia, Y. Lou, M. Gonin, J. B. Natowitz, R. Billerey, B. Cheynis, A. Demeyer, D. Drain, D. Guinet, C. Pastor, L. Vagneron, K. Zaid, J. Alarja, A. Giorni, D. Heuer, C. Morand, B. Viano, C. Mazur, C. Ngo, S. Leray, R. Lucas, M. Ribrag, and E. Tomasi, *Phys. Rev. C* **39**, 497 (1989).
- [20] D. Fox, D. A. Cebra, J. Karn, C. Parks, A. Pradhan, A. Vander Molen, J. van der Plicht, G. D. Westfall, W. K. Wilson, and R. S. Tickle, *Phys. Rev. C* **38**, 146 (1988).
- [21] H. C. Chiang and J. Hufner, *Nucl. Phys.* **A349**, 466 (1980).
- [22] I. Cervesato, E. Fabrici, E. Gadioli, E. Gadioli-Erba, and M. Galmarini, *Phys. Rev. C* **45**, 2369 (1992).
- [23] R. J. Glauber, *Phys. Rev.* **100**, 242 (1955).
- [24] D. R. Bowman, N. Colonna, W. A. Friedman, L. Celano, M. D'Agostino, J. D. Dinius, A. Ferrero, C. K. Gelbke, T. Glasmacher, D. O. Handzy, D. Horn, W. C. Hsi, M. Huang, I. Iori, M. A. Lisa, W. G. Lynch, G. V. Margagliotti, P. M. Milazzo, C. P. Montoya, A. Moroni, G. F. Peaslee, L. Phair, F. Petruzzelli, R. Scardaoni, C. Schwarz, M. B. Tsang, and C. Williams, *Phys. Rev. C* **22**, 818 (1995).
- [25] N. Marie, A. Chbihi, J. B. Natowitz, A. Le Fèvre, S. Salou, J. P. Wieleczko, L. Gingras, M. Assenard, G. Auger, Ch. O. Bacri, F. Bocage, B. Borderie, R. Bougault, R. Brou, P. Buchet, J. L. Charvet, J. Cibor, J. Colin, D. Cussol, R. Dayras, A. Demeyer, D. Doré, D. Durand, P. Eudes, J. D. Frankland, E. Galichet, E. Genouin-Duhamel, E. Gerlic, M. Germain, D. Gourio, D. Guinet, K. Hagel, P. Lantesse, J. L. Laville, J. F. Lecomte, T. Lefort, R. Legrain, N. Le Neindre, O. Lopez, M. Louvel, Z. Majka, A. M. Maskay, L. Nalpas, A. D. Nguyen, M. Parlog, J. Péter, E. Plagnol, A. Rahmani, T. Reposeur, M. F. Rivet, E. Rosato, F. Saint-Laurent, J. C. Steckmeyer, M. Stern, G. Tabacaru, B. Tamain, O. Tittel, E. Vient, C. Volant, and R. Wada, *Phys. Rev. C* **58**, 256 (1998).
- [26] S. Hudan, A. Chbihi, J. D. Frankland, A. Mignon, J. P. Wieleczko, G. Auger, N. Bellaïze, B. Borderie, A. Botvina, R. Bougault, B. Bouriquet, A. M. Buta, J. Colin, D. Cussol, R. Dayras, D. Durand, E. Galichet, D. Guinet, B. Guiot, G. Lanzalone, P. Lantesse, F. Lavaud, J. F. Lecomte, R. Legrain, N. Le Neindre, O. Lopez, L. Manduci, J. Marie, L. Nalpas, J. Normand, M. Pârlog, P. Pawowski, M. Pichon, E. Plagnol, M. F. Rivet, E. Rosato, R. Roy, J. C. Steckmeyer, G. Tbcaru, B. Tamain, A. van Lauwe, E. Vient, M. Vigilante, and C. Volant, *Phys. Rev. C* **67**, 06463 (2003).
- [27] R. Trockel, K. D. Hildenbrand, U. Lynen, W. F. J. Müller, H. J. Rabe, H. Sann, H. Stelzer, W. Trautmann, R. Wada, E. Eckert, P. Kreuz, A. Kühmichel, J. Pochodzalla, and D. Pelte, *Phys. Rev. C* **39**, 729 (1989).
- [28] J. A. Hauger, B. K. Srivastava, S. Albergo, F. Bieser, F. P. Brady, Z. Caccia, D. A. Cebra, A. D. Chacon, J. L. Chance, Y. Choi, S. Costa, J. B. Elliott, M. L. Gilkes, A. S. Hirsch, E. L. Hjort, A. Insolia, M. Justice, D. Keane, J. C. Kintner, V. Lindenstruth, M. A. Lisa, H. S. Matis, M. McMahan, C. McParland, W. F. J. Miller, D. L. Olson, M. D. Partlan, N. T. Porile, R. Potenza, G. Rai, J. Rasmussen, H. G. Ritter, J. Romanski, J. L. Romero, G. V. Russo, H. Sann, R. P. Scharenberg, A. Scott, Y. Shao, T. J. M. Symons, M. Tincknell, C. Tuvè, S. Wang, P. Warren, H. H. Wieman, T. Wienold, and K. Wolf, *Phys. Rev. C* **62**, 024616 (2000).
- [29] K. B. Morley, K. Kwiatkowski, D. S. Bracken, E. Renshaw Foxford, V. E. Viola, L. W. Woo, N. R. Yoder, R. Legrain, E. C. Pollacco, C. Volant, R. G. Korteling, H. Breuer, and J. Brzychczyk, *Phys. Rev. C* **54**, 737 (1996).
- [30] Y. D. Kim, R. T. de Souza, D. R. Bowman, N. Carlin, C. K. Gelbke, W. G. Gong, W. G. Lynch, L. Phair, M. B. Tsang, and F. Zhu, *Phys. Rev. C* **45**, 338 (1992).
- [31] M. Famiano *et al.*, *Phys. Rev. Lett.* **97**, 052701 (2006).

- [32] T. Keutgen *et al.* (unpublished data).
- [33] S. Albergo, S. Costa, E. Costanzo, and A. Rubbino, *Nuovo Cimento A* **89**, 1 (1985).
- [34] H. S. Xu, M. B. Tsang, T. X. Liu, X. D. Liu, W. G. Lynch, W. P. Tan, G. Verde, A. Vanderمولen, A. Wagner, H. F. Xi, C. K. Gelbke, L. Beaulieu, B. Davin, Y. Laroche, T. Lefort, R. T. de Souza, R. Yanez, V. Viola, R. J. Charity, and L. G. Sobotka, *Phys. Rev. Lett.* **85**, 716 (2000).
- [35] M. Veselsky, R. W. Ibbotson, R. Laforest, E. Ramakrishnan, D. J. Rowland, A. Ruangma, E. M. Winchester, E. Martin, and S. J. Yennello, *Phys. Rev. C* **62**, 041605 (2000).
- [36] H. Müller and B. Serot, *Phys. Rev. C* **52**, 2072 (1995).
- [37] V. Baran, M. Colonna, M. Di Toro, and A. B. Larioinov, *Nucl. Phys.* **A632**, 287 (1998).
- [38] L. G. Sobotka, J. F. Dempsey, R. J. Charity, and P. Danielewicz, *Phys. Rev. C* **55**, 2109 (1997).
- [39] J. B. Natowitz, R. Wada, K. Hagel, T. Keutgen, M. Murray, Y. G. Ma, A. Makeev, L. Qin, P. Smith, and C. Hamilton, *Phys. Rev. C* **65**, 034618 (2002).
- [40] M. A. Preston, *Physics of the Nucleus* (Addison-Wesley, Reading, MA, 1962).
- [41] J. B. Natowitz, K. Hagel, Y. Ma, M. Murray, L. Qin, S. Shlomo, R. Wada, and J. Wang, *Phys. Rev. C* **66**, 031601 (2002).
- [42] M. Beyer, S. A. Sofianos, C. Kuhrtz, G. Roepke, and P. Schuck, *Phys. Lett.* **B488**, 247 (2000).
- [43] H. Shen, H. Toki, K. Oyamatsu, and K. Sumiyoshi, *Nucl. Phys.* **A637**, 435 (1998); *Prog. Theor. Phys.* **100**, 1013 (1998).
- [44] C. J. Horowitz and A. Schwenk, *Nucl. Phys.* **A776**, 55 (2006).